Assessment of Cell Line Models of Primary Human Cells by Raman Spectral Phenotyping

Robin J. Swain,[†] Sarah J. Kemp,[§] Peter Goldstraw,[¶] Teresa D. Tetley,[§*] and Molly M. Stevens[†‡*]
[†]Department of Materials, [‡]Institute of Biomedical Engineering, [§]Lung Cell Biology, National Heart and Lung Institute, Imperial College London; and [¶]Department of Thoracic Surgery, Royal Brompton and Harefield National Health Service Foundation Trust, London, United Kingdom

ABSTRACT Researchers have previously questioned the suitability of cell lines as models for primary cells. In this study, we used Raman microspectroscopy to characterize live A549 cells from a unique molecular biochemical perspective to shed light on their suitability as a model for primary human pulmonary alveolar type II (ATII) cells. We also investigated a recently developed transduced type I (TT1) cell line as a model for alveolar type I (ATI) cells. Single-cell Raman spectra provide unique biomolecular fingerprints that can be used to characterize cellular phenotypes. A multivariate statistical analysis of Raman spectra indicated that the spectra of A549 and TT1 cells are characterized by significantly lower phospholipid content compared to ATII and ATI spectra because their cytoplasm contains fewer surfactant lamellar bodies. Furthermore, we found that A549 spectra are statistically more similar to ATI spectra than to ATII spectra. The spectral variation permitted phenotypic classification of cells based on Raman spectral signatures with >99% accuracy. These results suggest that A549 cells are not a good model for ATII cells, but TT1 cells do provide a reasonable model for ATI cells. The findings have far-reaching implications for the assessment of cell lines as suitable primary cellular models in live cultures.

INTRODUCTION

Research into various diseases, such as cancer, often relies on identifying drugs that influence cell growth and metabolism, or induce cell death (1). Stem-cell-based therapies in the context of regenerative medicine (2) and tissue engineering (3) rely on understanding how cells differentiate and interact with other cells, tissues, and materials. Primary stem, progenitor, and lineage-specific cells are the gold standards for studying cell growth and behavior in vitro. However, the use of primary cells can be hampered by an unreliable supply, the difficulty of performing isolation and culture procedures in vitro, and loss of phenotype with increasing time in culture. For example, primary pulmonary alveolar type II (ATII) epithelial cells lose their distinctive phenotype over a period of 1–2 weeks when cultured in vitro, as they undergo spontaneous differentiation resulting in expression of features characteristic of alveolar type I (ATI) cells (4).

To overcome these limitations, cell lines are often used as models for primary cells. These cells are typically derived from cancerous tissue or by immortalization of primary cells through retroviral transfection or transduction (5). Cell lines are generally easier to culture than primary cells, have a high proliferation rate and long lifespan, and maintain their phenotype in culture. However, the main disadvantage of cell lines is that the phenotype they express may not be consistent with the true phenotype of their primary counterparts (6).

The human A549 adenocarcinoma cell line has been used in lung cell biology as a model for ATII cells. These highly specialized cells produce surfactant, a multifunctional lubricant that reduces surface tension and prevents alveolar collapse during ventilation. The A549 cell line was derived from a type II pneumocyte lung tumor by Giard et al. in 1972 (7), and expresses some characteristic features of ATII cells, including synthesis of phospholipids, cytoplasmic lamellar bodies (Lbs), and apical microvilli (8). Since then, A549 cells have been used for in vitro studies of surfactant production and regulation of surfactant systems (9). However, the architecture and barrier properties of A549 cells are quite distinct from those of ATII cells (10), and, unlike primary ATII cells, cultured A549 cells do not undergo a transition to express an ATI-like phenotype. These differences, along with inconsistencies regarding A549 expression of ATII-specific markers, have led researchers to question the suitability of this cell line as an appropriate model for primary ATII cells (11).

In a recent study, we used Raman microspectroscopy to noninvasively characterize the in vitro differentiation of primary ATII cells to ATI cells (12). Raman microspectroscopy is a laser-based analytical technique that enables chemical characterization of molecules within a sample. It is a nondestructive optical technique based on the inelastic scattering of photons by molecular bond vibrations (13). A small fraction of photons are scattered by interaction with chemical bonds, resulting in a shift toward lower frequencies. The energy differences between incident and scattered photons correspond to specific vibrational energies of chemical bonds of the scattering molecules. The Raman spectrum of a cell represents an intrinsic biochemical fingerprint that contains molecular-level information about all cellular biopolymers. Raman spectroscopy has advantages over conventional cytochemical techniques because it allows rapid, noninvasive sensing, and the weak Raman scattering

Submitted August 6, 2009, and accepted for publication December 9, 2009.
*Correspondence: t.tetley@imperial.ac.uk or m.stevens@imperial.ac.uk
Editor: Leonid S. Brown.

0006-3495/10/04/1703/9 $2.00
doi: 10.1016/j.bpj.2009.12.4289

of aqueous media permits in vitro analysis of living cells in the absence of fixatives or labels (14). And whereas most biological assays probe for only a single marker, Raman spectroscopy simultaneously probes all molecular moieties. Furthermore, since Raman spectra are sensitive to changes in molecular composition, they can be used as cell-specific biochemical signatures to discriminate between different cellular phenotypes. Noninvasive spectral analysis has been used to identify cancer cells to aid in disease detection (15), as a biosensor to monitor cellular response to pharmaceuticals (16) and in vitro osteogenesis (17), and as a cytology tool to investigate cellular organelles (18), biochemistry (19), apoptosis (20), and differentiation (21).

In this study, we used Raman microspectroscopy for live cell culture analysis to compare the A549 phenotype with that of primary human ATII cells. We also investigated an immortal alveolar type I-like cell line (transduced type I (TT1)) that was recently developed and characterized by Kemp et al. (22) as a model for ATI cells. A549 and TT1 cells were tested for expression of ATII-specific (alkaline phosphatase (ALP), pro-surfactant protein C (pro-SPC)), and ATI-specific (caveolin-1) markers to correlate Raman spectral profiles with cellular phenotype. We used several well-established chemometric techniques, including principal components analysis (PCA), linear discriminant analysis (LDA), and spectral modeling to identify spectral markers that describe the biochemical differences between primary pulmonary alveolar epithelial cells and their model cell lines.

MATERIALS AND METHODS

Cell culture, cytochemical staining, and immunoblotting

Cells were cultured in media appropriate to each cell type, as surmised from previous studies within our laboratory and relevant studies within the literature. Primary human ATII cells were isolated and cultured as described previously (23). For staining and immunoblotting, purified ATII cells (0.75×10^6 cells/mL) were cultured on collagen type-I (1% (w/v) Vitrogen-100 (Imperial Laboratories, Andover, UK) in sterile deionized water, dried overnight) coated plates in defined cell culture medium 1 (DCCM-1; React Scientific, Ayr, UK) containing 10% (v/v) newborn calf serum, 100 U/mL penicillin, 100 μg/mL streptomycin, and 2 mM glutamine. The dilute collagen coating was used to promote cellular attachment and is unlikely to influence the analytical results. For characterization by Raman microspectroscopy, ATII cells (0.20×10^6 cells/mL) were cultured on collagen type-I coated MgF_2 coverslips (Global Optics, Bournemouth, UK) in DCCM-1, with supplements as above. MgF_2 is a weak Raman scatterer and is commonly used as a cell culture substrate for Raman spectroscopy (24). A lower seeding density was used for MgF_2 to facilitate collection of spectra from individual cells.

Human A549 lung carcinoma cells (American Type Culture Collection, Manassas, VA) were cultured in Dulbecco's modified Eagle's medium (DMEM) supplemented with 10% (v/v) fetal bovine serum (Invitrogen, Paisley, UK) and 1% (v/v) antibiotic/antimycotic (A/A; Invitrogen). Immortal TT1 cells were obtained by retroviral transduction of ATII cells as described by Kemp et al. (22), and cultured in DCCM-1 supplemented with 0.5 mg/mL G418 (Sigma, Dorset, UK). Cell lines were grown to 70% confluence before seeding (1.0×10^4 cells/mL) onto sterilized MgF_2 coverslips (not collagen-coated).

Staining for Lbs, ALP, and pro-SPC, and immunoblotting of caveolin-1 were performed as described previously (25,26). Additional details are provided in the Supporting Material.

Raman microspectroscopy

Raman spectra were measured with a Renishaw InVia spectrometer (Renishaw, Wotton-under-Edge, Gloucestershire, UK) connected to a Leica microscope (Leica, Wetzlar, Germany), as described previously (12). A high-power 785 nm diode line focus laser (~50 mW at the sample) was focused on cells by a 63× (NA = 0.9) long working distance (2 mm) water immersion objective (Leica). Under these conditions, the laser illuminates an elliptical region at the focal plane (10 μm × 20 μm lateral spatial resolution). The use of near-infrared radiation permits the use of high laser powers for nondestructive cellular analysis (24,27). Spectra of living cells were measured in DMEM with 1% (v/v) A/A at 37°C. Cells were serum-starved overnight for synchronization in the G_0/G_1 phase of the cell cycle to minimize cell-cycle-related spectral variance (28). Individual spectra were recorded for 40 s at a resolution of ~1–2 cm^{-1}. Raman backscattered radiation was directed through a holographic notch filter and 50 μm slit into the spectrometer (1200 lines/mm grating) before detection with a deep-depletion charge-coupled device detector.

Undifferentiated ATII cells were analyzed 3–4 days postseeding, and differentiated ATI cells were analyzed on days 10–11 and 17–18 postseeding. Two-day time points were used to allow analysis of sufficient cell numbers. Raman spectra of A549 and TT1 cells were collected between 72 and 96 h postseeding. Cells were characterized by computing the average spectra from multiple measurements per cell, and all efforts were taken to minimize the potential for overlap artifacts during signal collection.

Data analysis

All Raman data were analyzed with software developed in-house for MatLab (The Mathworks, Natick, MA). Spectra were intensity-corrected for instrument response (24), normalized with extended multiplicative signal correction (EMSC) (29), and smoothed using a Savitsky-Golay filter (five points, second-order polynomial), with the wavenumber axis aligned to the sharp phenylalanine peak at 1003 cm^{-1} and truncated to 600–1800 cm^{-1}. EMSC also correct spectra for variable background signal.

A least-squares fitting procedure was used to estimate the signal contribution of biochemical components to cellular Raman spectra, as described previously (12). Each mean cell spectrum was modeled by a linear combination of basis spectra representative of cellular biochemical components (Fig. S1), including nucleic acids (DNA and RNA), proteins (actin, human serum albumin, chymotrypsin, and collagen), carbohydrates (glycogen), and lipids (phosphatidyl choline (PCh) and cholesterol). A fifth-order polynomial was used to model the background signal, which can be attributed to scattering from DMEM culture medium and MgF_2 substrate, and fluorescence from aromatic compounds (16). To assess the quality of the fit, we compared the model spectra with the empirical data by examining residuals and computing correlation coefficients. The correlation coefficient provides a statistical measure of the similarity between spectra (30), and was used here as a goodness-of-fit parameter ($R = 1$ for identical spectral profiles).

PCA is a data compression algorithm that can be used to express high-dimensional spectra in terms of a small number of principal components (PCs) (31). PCs are orthogonal eigenvectors of the data covariance matrix, with the greatest variance captured by PC1, the second-greatest variance captured by PC2, etc. As such, the PCs form a set of basis spectra, and PC score values are weighting coefficients that describe the contribution of PCs to the original data. When applied to Raman spectra, PCs contain spectral features corresponding to the main molecular species responsible for the statistical variation between spectra. We carried out separate two-group comparisons: one between ATII and A549 cells, and one between

ATI and TT1 cells. In each case, only spectra of cells within the two groups being compared were included in the PCA. In addition, we also performed a four-group PCA that incorporated spectra of all four cell types.

LDA is a supervised classification algorithm for discrimination of sample groups. The algorithm computes linear discriminant functions that maximize the ratio of between-class variance to within-class variance according to Fisher's criterion (32). Since LDA requires fewer variables than observations, PCA was used to compress the spectra and the PC scores were used as input for LDA. We assessed the accuracy of classification using the leave-one-out cross-validation method, whereby the class of a spectrum is predicted by means of an LDA model built from the full data set, excluding the spectrum in question. This method is repeated, with each spectrum left out in turn, so that the class of each spectrum is predicted once.

RESULTS

Cytochemical characterization of lung cell phenotypes

Differentiation of primary ATII cells proceeded as described previously (12). Undifferentiated ATII cells were cuboidal, stained positive for ATII-specific cell markers Lbs (Fig. 1 *A*), ALP, and pro-SPC, and only weakly expressed caveolin-1, an ATI-specific marker (Fig. S2). With increasing time in culture, the cells adopted a flattened morphology with a raised perinuclear region and thin cytoplasmic attenuations. The staining pattern at later time points shifted to a strong expression of caveolin-1 and a weak expression of ALP, pro-SPC, and Lbs, confirming the spontaneous differentiation of ATII cells to an ATI cell phenotype in vitro.

For the cell lines, no differences in growth, morphology, or expression of phenotypic markers were observed between MgF_2 and tissue culture substrates. The A549 cells typically were small and cuboidal, and stained positive for numerous Lbs (Fig. 1 *C*), although Lb staining was less intense and uniform than observed in ATII cells (Fig. 1 *A*). TT1 cell morphology was similar to that of ATI cells, but TT1 cells were less squamous and thin cytoplasmic attenuations were less prevalent. Lb staining was weakest in TT1 cells (Fig. 1 *D*), and neither A549 nor TT1 cells expressed ALP or pro-SPC (Fig. S2, *A* and *B*). Immunoblotting revealed positive expression of caveolin-1 in cultures of TT1 cells, although at lower levels than observed in ATI cell cultures. Caveolin-1 expression by A549 cells was extremely weak or negative (Fig. S2 *C*).

Spectral variability within cells

We measured Raman spectra at different positions in each cell to study spectral variation with respect to subcellular location. Similar patterns of spectral heterogeneity were observed in all cell types, and in general, cytoplasm spectra exhibited stronger lipid vibrations than spectra collected from cell nuclei, which were dominated by protein and nucleic acid spectral features. The strong phospholipid vibrations observed in the cytoplasm spectra (Fig. 2) are due to the presence of surfactant-containing Lbs in all cell types.

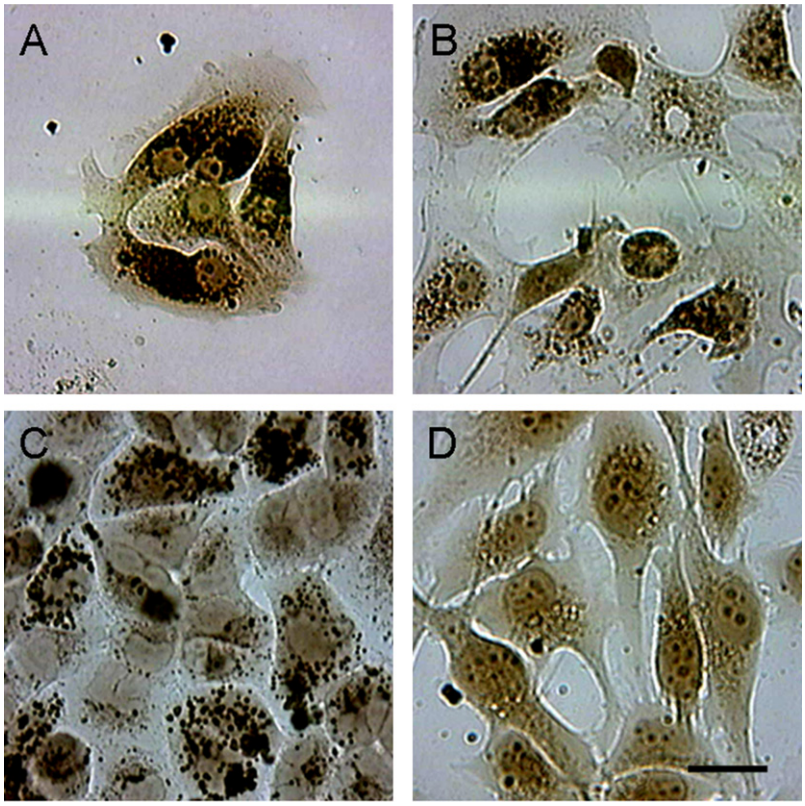

FIGURE 1 Morphology of cells cultured on MgF_2 coverslips. Light-microscope images of (*A*) ATII, (*B*) ATI, (*C*) A549, and (*D*) TT1 cells stained for Lbs with osmium tetroxide and tannic acid. Dark osmiophilic granules indicate cytoplasmic Lbs. Scale bar = 20 μm.

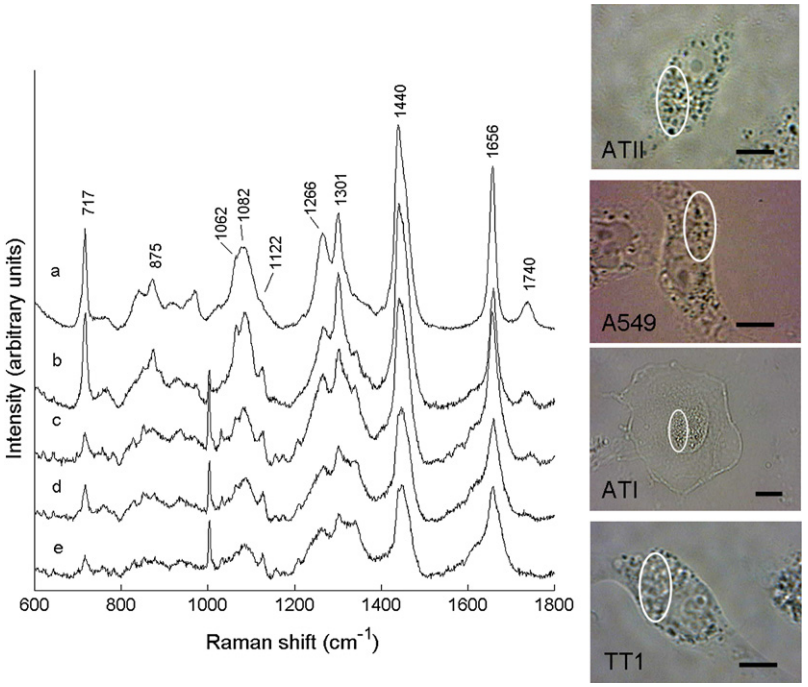

FIGURE 2 Raman spectrum of PCh (*line a*); typical Raman spectra collected from the cytoplasm of ATII cells (*line b*), A549 cells (*line c*), ATI cells (*line d*) and TT1 cells (*line e*). Spectra have been corrected for instrument response, EMSC normalized, baseline-corrected, wavenumber alignment, and vector normalized. Light microscope pictures indicate the region probed by each scan. Spectra are offset for clarity. Scale bar = 10 μm. Correlation coefficients between the PCh spectrum and ATII, A549, ATI, and TT1 cytoplasm spectra shown are $R = 0.970$, 0.889, 0.859, and 0.817, respectively.

Biomolecular characterization of single living cells

ATII cells had typical dimensions of ~20 μm × 30 μm, and we found that three spectra were adequate to probe single ATII cells. Spectra of the perinuclear region of ATI cells demonstrated high intensity and a good signal/noise ratio, whereas those of the thin cytoplasmic attenuations were weak and noisy, and did not display significant features above the signal of the culture medium. Therefore, our analysis of ATI cells was based on perinuclear cellular regions only, which were similar in size to ATII cells (12). Thus, the mean spectra representing the biomolecular fingerprints of individual ATII and ATI cells were based on three spectral measurements per cell. A549 and TT1 cells were typically larger than ATII cells and their size was more variable; therefore, mean A549 and TT1 cell spectra were computed from three to five measurements per cell, depending on cell size and shape.

The average processed Raman spectra of all ATII and A549 cells are shown in Fig. 3 *A*, and those of ATI and TT1 cells are shown in Fig. 3 *B*. The *solid black lines* denote average spectra, which represent the mean of 183, 250, 375, and 222 spectra collected from 61 ATII, 57 A549, 125 ATI, and 56 TT1 cells, respectively. The small standard deviations (SDs; *gray lines*) within each group indicate that Raman spectral characterization of lung cell phenotypes is highly reproducible. The spectra consist of peaks corresponding to molecular vibrations of all cellular biopolymers. Specific assignments of individual peaks, compiled from previous studies (12,18,24), are presented in Table S1. Scatterplots of the intensity values of the main peaks that differ between spectra of primary cells and cell lines are shown in Fig. S3. All peaks indicated in Fig. 3 have significantly different ($p < 0.05$) mean intensities, determined using the Mann-Whitney test. The lack of sharp, derivative-like peak features in the difference spectra (ATII-A549 and ATI-TT1) of Fig. 3 indicate that no shifting of major Raman bands was observed in the spectra of the different cell types reported here.

Spectral modeling

We fit the mean spectra of individual lung cells with a set of basis spectra modeling cellular biochemical components using a nonnegative least-squares fitting routine. Examples of the fitting results are displayed in Fig. 4, where the mean overall spectra of ATII, A549, ATI, and TT1 cells are plotted along with the model-predicted spectra and residuals. Low-intensity residual spectra and high correlation coefficients obtained for all ATII ($R_{mean} = 0.995 \pm 0.002$), A549 ($R_{mean} = 0.995 \pm 0.003$), ATI ($R_{mean} = 0.994 \pm 0.002$), and TT1 cells ($R_{mean} = 0.993 \pm 0.002$) indicate that the least-squares model provides a good fit to the data.

To determine the signal contributions of the biochemical components to cellular spectra, we normalized the model fit coefficients for each individual cell to unity sum, and calculated the mean ± SDs for each cell type (Table 1). The results are grouped together in terms of component classification (nucleic acids, proteins, carbohydrates, and lipids) because, despite the presence of some distinct peaks within component spectra, the nonorthogonal nature of similar basis spectra prevents spectral resolution of individual components (33). Differences in normalized fit coefficients between

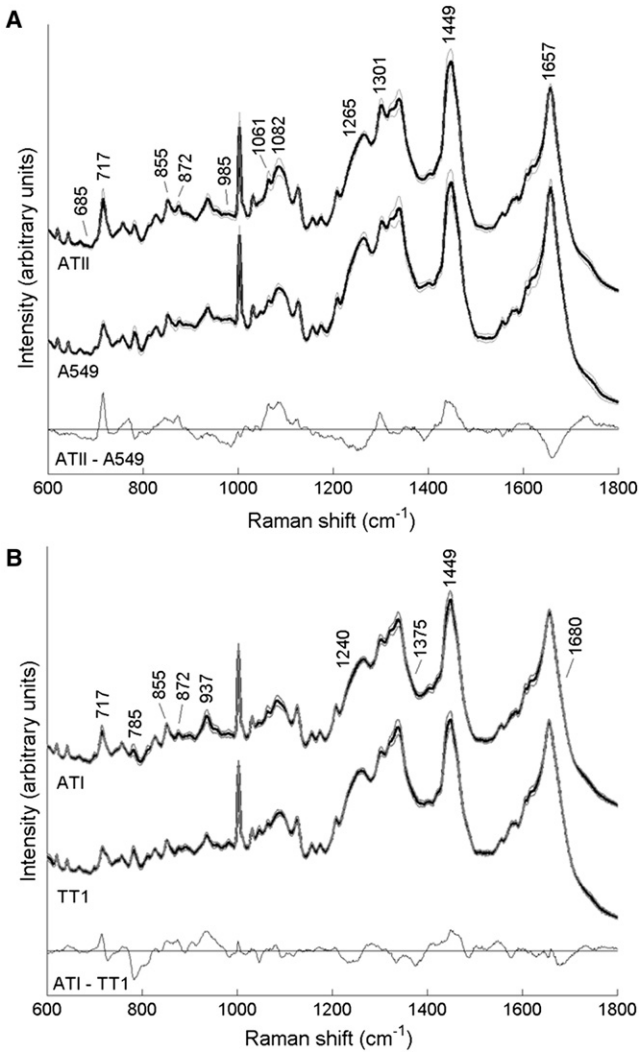

FIGURE 3 Average Raman spectra of (*A*) ATII and A549 cells, and (*B*) ATI and TT1 cells. Solid black lines denote average spectra, and gray lines delineate 1 SD. Spectra are offset for clarity. Difference spectra (ATII-A549 and ATI-TT1) are also included (magnified by a factor of 2.5).

primary cells and cell lines were tested for statistical significance using the Mann-Whitney test.

PCA

PCA was performed on the mean Raman spectra of individual lung cells. A PC-score plot is a bivariate scatterplot in which data are depicted in terms of spectral coordinates. These plots facilitate comparison of different cell types (clustering or grouping within score plots indicates systematic differences between groups of spectra). Direct two-group comparisons between ATII/A549 and ATI/TT1 cells are presented in Fig. 5, *A* and *B*, respectively. We also performed a PCA on the entire data set to compare all four cell types (Fig. S4). The size and position of cell clusters in the four-group PCA are indicated in Fig. 5 *C*. Details of the percent variance described by each plot are provided in the figure captions.

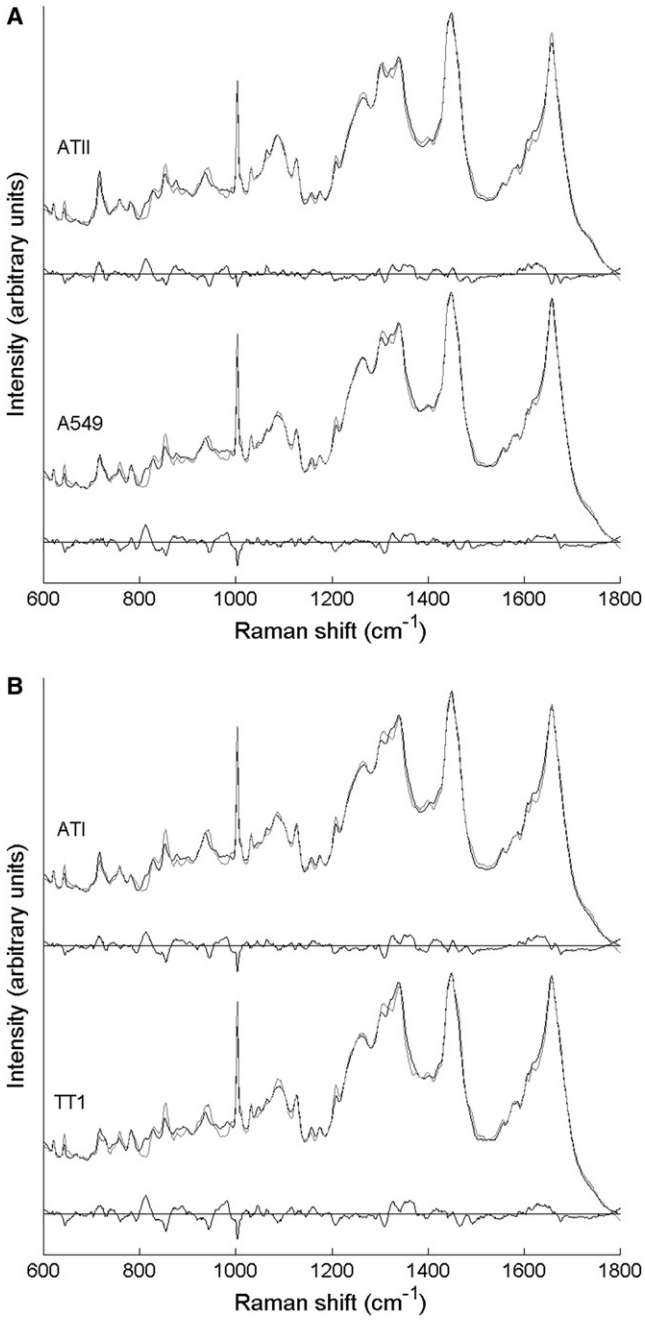

FIGURE 4 Spectral modeling of (*A*) ATII and A549 cells, and (*B*) ATI and TT1 cells. Mean spectra are shown in black, model fits in gray, and residual spectra in black, offset for clarity. Correlation coefficients between the mean and model spectra shown are $R = 0.996$, 0.997, 0.996, and 0.994, respectively.

LDA

PC-score plots are two-dimensional projections of high-dimensional spectral data, and discrimination is based on a limited portion of the total variance. LDA is an extension of PCA that incorporates much more spectral variance as well as class membership of data to produce maximal group separation. To determine whether ATII and A549 cells could

TABLE 1 Relative percent signal contribution of model basis components to cellular Raman spectra

Cell type	Nucleic acid (%)	Protein (%)	CHO* (%)	Lipid (%)
ATII ($n = 61$)	11.8 ± 2.0	51.8 ± 7.7	8.5 ± 1.6	27.9 ± 8.8
A549 ($n = 57$)	11.6 ± 3.5	61.1 ± 5.7†	5.5 ± 2.4†	21.7 ± 9.0†
ATI ($n = 125$)	9.7 ± 2.9	62.1 ± 5.2	9.3 ± 1.2	18.9 ± 6.5
TT1 ($n = 56$)	15.0 ± 2.1‡	61.0 ± 3.9‡	8.4 ± 1.5‡	15.7 ± 5.9‡

*CHO = carbohydrate.
† and ‡ denote statistically significant differences between ATII/A549 and ATI/TT1 cells, respectively (computed using the Mann-Whitney test, $p < 0.05$).

be distinguished solely by their Raman spectra, we used the scores on the first 25 PCs (accounting for 96.2% of variance) generated in the direct ATII-A549 comparison to develop an LDA classification model. A separate 25-PC model (accounting for 94.3% of variance) was developed to distinguish between spectra of ATI and TT1 cells. PC-LDA models were obtained by starting with two PCs and incorporating additional PCs until data classification was optimal.

Cross-validation of the ATII-A549 LDA model revealed 100% sensitivity and specificity for both cell types, with all 61 ATII and 57 A549 cells classified correctly. In the ATI-TT1 LDA model cross-validation, all 56 TT1 cells and 124/125 ATI cells were classified correctly, yielding 99% sensitivity, 100% specificity for ATI cells, and 100% sensitivity, 98% specificity for TT1 cells.

DISCUSSION

The appropriate use of cell lines as models for primary cells is important in cancer research, stem cell research, and tissue engineering. As such, the degree to which the phenotype expressed by cell lines represents that of the primary system is of central relevance. The suitability of the A549 cell line as a model for ATII cells was initially questioned by Mason and Williams (11) in 1982, when they discovered that the surfactant produced by A549 cell cultures differed significantly from that of primary (murine) ATII cells. Since then, discrepancies regarding A549 cell expression of ATII-specific ultrastructural and cytochemical markers have led researchers to further question the stability and robustness of the A549 cell line. In contrast, a recently developed type I cell line (TT1) has been shown to express ATI-specific markers (22), and displays potential as a model for studying the biochemical and transport properties of primary ATI cells.

In this work, we aimed to scrutinize the appropriateness of A549 and TT1 cell lines as models for primary ATII and ATI cells, respectively. We used Raman microspectroscopy as a novel phenotypic characterization method to assess these models from a unique perspective, and by validating our results with gold-standard cytochemical techniques, we were able to obtain a more comprehensive view by which to judge the merits of the cell line models.

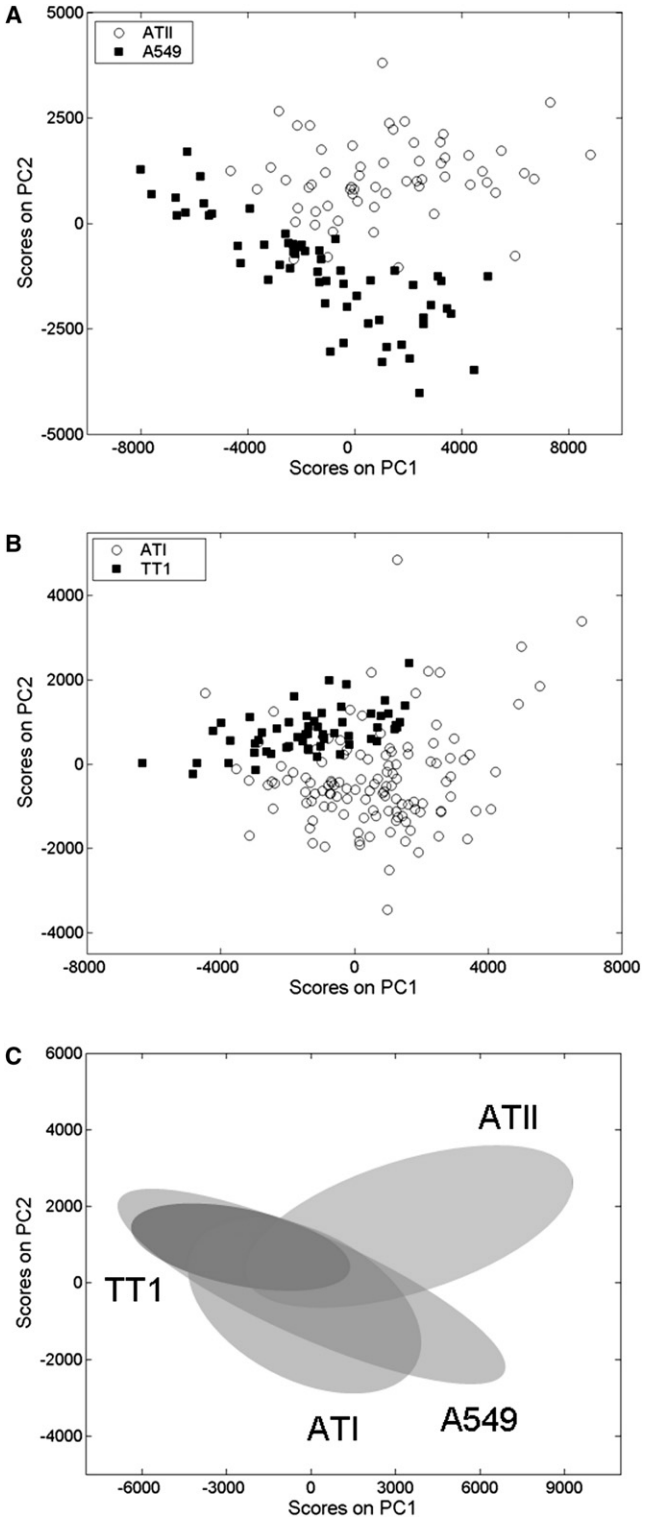

FIGURE 5 PC1-PC2 score plots. Direct PCA of (*A*) ATII versus A549 cells, and (*B*) ATI versus TT1 cells. These plots incorporate 73.7% (60.3% on PC1, 13.4% on PC2) of the variance between ATII and A549 cell spectra, and 59.5% (45.8% on PC1, 13.7% on PC2) of the variance between ATI and TT1 cell spectra. (*C*) Score plot from four-group PCA, as in Fig. S4, with shaded regions showing the position of all four data clusters (data points removed for clarity).

Cytochemical characterization of lung cell phenotypes

The A549 cell line has been extensively characterized (8,34) and used as a model for primary ATII cells. Although it was shown to produce phospholipids and stain positive for Lbs (34), several discrepancies with respect to A549 expression of ATII-specific markers are reported in the literature. Fuchs et al. (4) characterized A549 cells as expressing high levels of SPC and low levels of caveolin-1, indicating an ATII phenotype. This was supported by Campbell et al. (35), who reported that A549 cells lack caveolae and only weakly express caveolin-1 (both of which are ATI cell markers). However, Witherden et al. (25) did not detect expression of SPC or surfactant protein A mRNA by A549 cells. The A549 cultures examined here were negative for ALP (in agreement with McCormick et al. (36)) and pro-SPC, and weakly expressed both isoforms of caveolin-1 (Fig. S2 *C*), indicating significant differences between the phenotypes of A549 and ATII cells. With respect to other markers, Carolan and Casale (37) found that A549 cells demonstrate significantly lower transepithelial electrical resistance than primary ATII cells, Nakano et al. (38) reported strong expression of the ATI-specific marker receptor for advanced glycation end products, and Pechkovsky et al. (39) found significant differences in expression of nitric oxide synthase mRNA between ATII and A549 cells. It has been suggested that the conflicting results regarding A549 cells reflect inconsistencies among batches of A549 cells, possibly depending on culture conditions and passage number (25). The A549 cells examined here clearly express some phenotypic features of both primary ATII cells (positive Lb stain, weak caveolin-1 expression) and ATI cells (negative staining for ALP and pro-SPC).

TT1 cell morphology was consistent with that of ATI cells, with weak staining for Lbs. Several vacuole-like structures were observed and could be reminiscent of residual or incomplete Lbs (4). In addition, TT1 cells did not stain positive for ALP or pro-SPC, but did express caveolin-1, albeit at a lower level than cultures of in vitro-derived ATI cells (Fig. S2 *C*). These results agree with the recent characterization of TT1 cells by Kemp et al. (22) and indicate that, based on the markers probed here, TT1 cells express an ATI-like phenotype. This was expected because the immortalized TT1 cell line was derived from cultures of primary ATII cells that had spontaneously differentiated toward an ATI phenotype (22), as occurs in vivo.

Raman spectral characterization of lung cell phenotypes

Biomolecular characterization of lung cells with Raman microspectroscopy revealed that both primary cells and cell lines exhibit variation between lipid-rich cytoplasm spectra and protein/nucleic acid-dominated nucleus spectra. Correlation coefficients between the spectrum of PCh and ATII cytoplasm spectra (Fig. 2) were typically much higher than those computed for ATI, A549, and TT1 cytoplasm spectra, confirming a significantly higher contribution of phospholipid molecular vibrations to ATII cytoplasm spectra. This is due to a higher concentration of phospholipid-rich Lbs in the cytoplasm of ATII cells (Fig. 1).

An average Raman spectrum was computed for each cell to compare cellular biomolecular signatures within and between groups of ATII, A549, ATI, and TT1 cells. Raman analysis produced highly reproducible and informative spectra. The small SDs about the mean spectra (Fig. 3, *A* and *B*, *gray lines*) suggest consistent phenotypic characterization with Raman microspectroscopy. This was expected for immortalized and cancer cell lines, but surprisingly was also observed within cultures of primary ATII and ATI cells, reflecting the high ATII cell purity (~95%) afforded by our isolation protocol (23).

The main differences between the spectra of ATII and A549 cells are highlighted by the difference spectrum in Fig. 3 *A* and the scatterplot in Fig. S3 *A*. Mean ATII cell spectra had significantly stronger peaks corresponding to phospholipid vibrations (717, 872, 1061, 1082, and 1301 cm^{-1}), whereas peaks associated with protein vibrations (685 cm^{-1}, 985 cm^{-1}, extended amide III band ~1265 cm^{-1}) were more intense in the spectra of A549 cells. Also, the amide I band (~1657 cm^{-1}) was broader in the spectra of A549 cells compared to ATII cells, indicating lower unsaturated phospholipid and higher protein content. These univariate peak observations were supported by multivariate spectral modeling (Table 1), which revealed on average a 6% higher phospholipid signal contribution to ATII spectra than to A549 spectra. In fact, the pattern of biochemical signal contribution to spectra of A549 cells had more similarity to ATI cells than to ATII cells. The protein signal contribution to mean A549 spectra was ~10% higher than for ATII spectra. The reason for the significant difference between carbohydrate signal content in the spectra of ATII and A549 cells is unclear at present, but may be an artifact of modeling complex cellular spectra with a limited number of nonorthogonal basis spectra. Furthermore, since the data are expressed as relative rather than absolute amounts, the reduced carbohydrate content in A549 spectra may simply reflect an increase in one or more of the other cellular constituents.

The significant differences between ATI and TT1 spectra indicated in Fig. 3 *B* and Fig. S3 *B* include variation in the molecular vibrations of phospholipids (717 cm^{-1}), proteins (855, 872, and 937 cm^{-1}, upper region of amide I band ~1680 cm^{-1}), nucleic acids (785 and 1375 cm^{-1}), as well as vibrations common to all molecular moieties (e.g., CH deformation vibrations at 1449 cm^{-1}). These findings were supported by spectral modeling, which revealed significant differences in the signal contributions of all biomolecular components to spectra of ATI and TT1 cells. In particular, the signal contribution of nucleic acids to TT1 spectra was

~5.3% higher than for ATI spectra, which could indicate a higher proliferation rate in the transduced cell line. In addition, the lipid signal contribution to TT1 spectra was significantly lower (by ~3%) than that to primary ATI spectra.

Spectral discrimination via PCA and LDA

The PCs contain spectral features that describe the biomolecular species responsible for discrimination of cell populations. In the data sets examined here, the biomolecular species implicated by the PC loading vectors were consistent with those identified by multivariate spectral modeling. The PC1-PC2 score plots in Fig. 5 depict clusters of cell populations, grouped on the basis of spectral similarity. The cluster patterns indicate that primary ATII and ATI cells cannot completely be distinguished from model A549 and TT1 cell lines with only two PCs. In particular, the observed variability among A549 cells was larger than initially expected, but is likely to reflect inconsistent phenotypic expression of A549 cells as discussed above. However, despite overlap in the PC score plots, the more sensitive LDA results demonstrate that one can discriminate between ATII/A549 cells and ATI/TT1 cells by incorporating additional spectral information (i.e., by using 25 PCs). The additional information enabled 100% spectral discrimination between ATII and A549 cells, and >99% classification accuracy of ATI and TT1 cells. The latter result, coupled with the distinct cluster centroids for ATI and TT1 cells shown in Fig. 5 *B*, suggests that, although they exhibit similar staining and immunoblotting patterns (Fig. 1 and Fig. S2), immortalized TT1 cells are spectrochemically distinct from their primary counterpart. This demonstrates the high sensitivity of Raman microspectroscopy in comparison with traditional cytochemical techniques for detecting cellular biochemical alterations induced by transduction. And, in contrast to the conflicting results of cytochemical experiments comparing A549 and ATII cells, our Raman-based analysis clearly identifies distinct biochemical differences between these cell types.

Interestingly, clustering in the combined PC1-PC2 score plot (Fig. S4) indicated that A549 spectra occupy a region similar to those of ATI and TT1 cells (Fig. 5 *C*). Thus, with respect to the common basis vectors PC1 and PC2, A549 spectra are more similar to spectra of ATI cells than those of ATII cells. These findings, supported by LDA and biochemical signal profiles determined by spectral modeling, suggest that A549 cells are not a good model for primary ATII cells, for if they were, we would expect A549 and ATII clusters to occupy a similar region within the PC1-PC2 score plot. In light of these findings and the inconsistency of the A549 phenotype, it is important to recognize the limitations of the A549 cell line as a substitute for ATII cells. The A549 cell line may be appropriate for use in cancer studies of adenocarcinoma, as a monolayer culture to mimic ATI cells in studies of solute transport (40), and as a model for dysfunctional ATII cells, as suggested by Balis et al. (41).

In contrast, our analysis suggests that the TT1 cell line provides a suitable model for ATI cells, exhibiting positive expression of ATI-specific markers and negative expression of ATII-specific markers. However, a multivariate statistical comparison of ATI and TT1 spectra did reveal key biochemical differences between these spectrochemically distinct cell types. This finding underscores the point that no model is perfect, and one should always bear the limitations of a particular model in mind when using it to represent a primary system.

CONCLUSIONS

Previous phenotypic characterizations of A549 cells by traditional cytochemical techniques have led to an inconsistent view as to whether they provide a suitable model for primary ATII cells. The results of Raman spectral phenotyping of ATII and A549 cells presented here cast further doubt on the use of A549 cells to represent ATII cells. The spectra of A549 cells were statistically more similar to those of differentiated ATI cells than to those of undifferentiated ATII cells, and we were able to achieve 100% spectral discrimination between ATII and A549 cells. In contrast to the shortcomings of the A549 cell line model of primary ATII cells, the recently developed TT1 cell line exhibits positive expression of ATI-specific markers and negative expression of ATII-specific markers, and thus provides a suitable model for ATI cells. A multivariate statistical comparison of ATI and TT1 cell spectra did, however, reveal key biochemical differences between these spectrochemically distinct cell types. These results suggest that investigators should give careful consideration to the limitations of cell lines when using them to model primary cells in biological applications.

SUPPORTING MATERIAL

Four figures and one table are available at http://www.biophysj.org/biophysj/supplemental/S0006-3495(09)06138-4.

We thank Dr. Kees Maquelin for assistance in processing the EMSC data, and Dr. Gavin Jell for proofreading the manuscript.

This study was supported in part by the Leverhulme Trust. R.J.S. received financial support from the Rothermere Trust Foundation, National Science and Engineering Research Council (Canada), and Canadian Centennial Scholarship Fund. S.J.K. received funding from the Department of Health (United Kingdom). This project was supported by the National Institute for Health Research Respiratory Disease Biomedical Research Unit at the Royal Brompton and Harefield National Health Service Foundation Trust and Imperial College London.

REFERENCES

1. Wang, S., and W. S. El-Deiry. 2004. Apoptosis signaling in normal and cancer cells. *In* Cell Cycle and Growth Control: Biomolecular Regulation and Cancer. G. S. Stein and A. B. Pardee, editors. John Wiley & Sons, Hoboken, NJ. 497–524.

2. Assmus, B., V. Schächinger, …, A. M. Zeiher. 2002. Transplantation of progenitor cells and regeneration enhancement in acute myocardial infarction (TOPCARE-AMI). *Circulation*. 106:3009–3017.
3. Langer, R., and J. P. Vacanti. 1993. Tissue engineering. *Science*. 260:920–926.
4. Fuchs, S., A. J. Hollins, …, C. M. Lehr. 2003. Differentiation of human alveolar epithelial cells in primary culture: morphological characterization and synthesis of caveolin-1 and surfactant protein-C. *Cell Tissue Res*. 311:31–45.
5. O'Hare, M. J., J. Bond, …, P. S. Jat. 2001. Conditional immortalization of freshly isolated human mammary fibroblasts and endothelial cells. *Proc. Natl. Acad. Sci. USA*. 98:646–651.
6. Clover, J., and M. Gowen. 1994. Are MG-63 and HOS TE85 human osteosarcoma cell lines representative models of the osteoblastic phenotype? *Bone*. 15:585–591.
7. Giard, D. J., S. A. Aaronson, …, W. P. Parks. 1973. In vitro cultivation of human tumors: establishment of cell lines derived from a series of solid tumors. *J. Natl. Cancer Inst*. 51:1417–1423.
8. Lieber, M., B. Smith, …, G. Todaro. 1976. A continuous tumor-cell line from a human lung carcinoma with properties of type II alveolar epithelial cells. *Int. J. Cancer*. 17:62–70.
9. Salmona, M., M. Donnini, …, M. Luisetti. 1992. A novel pharmacological approach for paraquat poisoning in rat and A549 cell line using ambroxol, a lung surfactant synthesis inducer. *Food Chem. Toxicol*. 30:789–794.
10. Godfrey, R. W. 1997. Human airway epithelial tight junctions. *Microsc. Res. Tech*. 38:488–499.
11. Mason, R. J., and M. C. Williams. 1980. Phospholipid composition and ultrastructure of A549 cells and other cultured pulmonary epithelial cells of presumed type II cell origin. *Biochim. Biophys. Acta*. 617: 36–50.
12. Swain, R. J., S. J. Kemp, …, M. M. Stevens. 2008. Spectral monitoring of surfactant clearance during alveolar epithelial type II cell differentiation. *Biophys. J*. 95:5978–5987.
13. Raman, C. V., and K. S. Krishnan. 1928. A new type of secondary radiation. *Nature*. 121:501–502.
14. Puppels, G. J., F. F. de Mul, …, T. M. Jovin. 1990. Studying single living cells and chromosomes by confocal Raman microspectroscopy. *Nature*. 347:301–303.
15. Crow, P., B. Barrass, …, N. Stone. 2005. The use of Raman spectroscopy to differentiate between different prostatic adenocarcinoma cell lines. *Br. J. Cancer*. 92:2166–2170.
16. Owen, C. A., J. Selvakumaran, …, M. M. Stevens. 2006. In vitro toxicology evaluation of pharmaceuticals using Raman micro-spectroscopy. *J. Cell. Biochem*. 99:178–186.
17. Gentleman, E., R. J. Swain, …, M. M. Stevens. 2009. Comparative materials differences revealed in engineered bone as a function of cell-specific differentiation. *Nat. Mater*. 8:763–770.
18. Matthäus, C., T. Chernenko, …, M. Diem. 2007. Label-free detection of mitochondrial distribution in cells by nonresonant Raman microspectroscopy. *Biophys. J*. 93:668–673.
19. van Manen, H. J., Y. M. Kraan, …, C. Otto. 2005. Single-cell Raman and fluorescence microscopy reveal the association of lipid bodies with phagosomes in leukocytes. *Proc. Natl. Acad. Sci. USA*. 102:10159–10164.
20. Verrier, S., I. Notingher, …, L. L. Hench. 2004. In situ monitoring of cell death using Raman microspectroscopy. *Biopolymers*. 74:157–162.
21. Notingher, I., I. Bisson, …, L. L. Hench. 2004. In situ spectral monitoring of mRNA translation in embryonic stem cells during differentiation in vitro. *Anal. Chem*. 76:3185–3193.
22. Kemp, S. J., A. J. Thorley, …, T. D. Tetley. 2008. Immortalization of human alveolar epithelial cells to investigate nanoparticle uptake. *Am. J. Respir. Cell Mol. Biol*. 39:591–597.
23. Witherden, I. R., and T. D. Tetley. 2001. Isolation and culture of human type II pneumocytes. *In* Human Airway Inflammation: Sampling Techniques and Analytical Protocols. D. F. Rogers and L. E. Donnelly, editors. Humana Press, Totawa, NJ. 127–136.
24. Notingher, I., G. Jell, …, L. L. Hench. 2004. In situ non-invasive spectral discrimination between bone cell phenotypes used in tissue engineering. *J. Cell. Biochem*. 92:1180–1192.
25. Witherden, I. R., E. J. Vanden Bon, …, T. D. Tetley. 2004. Primary human alveolar type II epithelial cell chemokine release: effects of cigarette smoke and neutrophil elastase. *Am. J. Respir. Cell Mol. Biol*. 30:500–509.
26. Alcorn, J. L., M. E. Smith, …, C. R. Mendelson. 1997. Primary cell culture of human type II pneumonocytes: maintenance of a differentiated phenotype and transfection with recombinant adenoviruses. *Am. J. Respir. Cell Mol. Biol*. 17:672–682.
27. Puppels, G. J., J. H. Olminkhof, …, J. Greve. 1991. Laser irradiation and Raman spectroscopy of single living cells and chromosomes: sample degradation occurs with 514.5 nm but not with 660 nm laser light. *Exp. Cell Res*. 195:361–367.
28. Swain, R. J., G. Jell, and M. M. Stevens. 2008. Non-invasive analysis of cell cycle dynamics in single living cells with Raman micro-spectroscopy. *J. Cell. Biochem*. 104:1427–1438.
29. Martens, H., J. P. Nielsen, and S. B. Engelsen. 2003. Light scattering and light absorbance separated by extended multiplicative signal correction. application to near-infrared transmission analysis of powder mixtures. *Anal. Chem*. 75:394–404.
30. Diem, M., M. Romeo, …, C. Matthaus. 2004. A decade of vibrational micro-spectroscopy of human cells and tissue (1994–2004). *Analyst (Lond.)*. 129:880–885.
31. Wold, S., K. Esbensen, and P. Geladi. 1987. Principal components analysis. *Chemom. Intell. Lab. Syst*. 2:37–52.
32. Hair, J. F., R. E. Anderson, R. L. Tatham, and W. C. Black. 1998. Multivariate Data Analysis. Prentice-Hall, Upper Saddle River, NJ.
33. Mourant, J. R., K. W. Short, …, J. P. Freyer. 2005. Biochemical differences in tumorigenic and nontumorigenic cells measured by Raman and infrared spectroscopy. *J. Biomed. Opt*. 10:031106.
34. Foster, K. A., C. G. Oster, …, K. L. Audus. 1998. Characterization of the A549 cell line as a type II pulmonary epithelial cell model for drug metabolism. *Exp. Cell Res*. 243:359–366.
35. Campbell, L., A. J. Hollins, …, M. Gumbleton. 1999. Caveolin-1 expression and caveolae biogenesis during cell transdifferentiation in lung alveolar epithelial primary cultures. *Biochem. Biophys. Res. Commun*. 262:744–751.
36. McCormick, C., R. I. Freshney, and V. Speirs. 1995. Activity of interferon α, interleukin 6 and insulin in the regulation of differentiation in A549 alveolar carcinoma cells. *Br. J. Cancer*. 71:232–239.
37. Carolan, E. J., and T. B. Casale. 1996. Neutrophil transepithelial migration is dependent upon epithelial characteristics. *Am. J. Respir. Cell Mol. Biol*. 15:224–231.
38. Nakano, N., K. Fukuhara-Takaki, …, R. Nagai. 2006. Association of advanced glycation end products with A549 cells, a human pulmonary epithelial cell line, is mediated by a receptor distinct from the scavenger receptor family and RAGE. *J Biochem*. 139:821–829.
39. Pechkovsky, D. V., G. Zissel, …, J. Müller-Quernheim. 2002. Pattern of NOS2 and NOS3 mRNA expression in human A549 cells and primary cultured AEC II. *Am. J. Physiol. Lung Cell. Mol. Physiol*. 282:L684–L692.
40. Kobayashi, S., S. Kondo, and K. Juni. 1995. Permeability of peptides and proteins in human cultured alveolar A549 cell monolayer. *Pharm. Res*. 12:1115–1119.
41. Balis, J. U., S. D. Bumgarner, …, S. A. Shelley. 1984. Synthesis of lung surfactant-associated glycoproteins by A549 cells: description of an in vitro model for human type II cell dysfunction. *Exp. Lung Res*. 6:197–213.